

# LOW -VOLTAGE LARGE ANGULAR DISPLACEMENT ELECTROSTATIC SCANNING MICROMIRROR USING FLOATING SLIDER MECHANISM

<sup>1</sup>Kerwin Wang, <sup>2</sup>Michael J. Sinclair and <sup>1</sup>Karl F. Böhringer

<sup>1</sup>Electrical Engineering Department, University of Washington, Seattle, WA, USA

<sup>2</sup>Microsoft Research, Redmond, WA, USA

## ABSTRACT

This paper presents a floating slider mechanism to achieve large scanning angular displacements with low voltage electrostatic mirrors. It can amplify the mirror angular displacement from the movement of bimorph electrostatic actuators. Depending on the actuator designs, the initial tilting angles of the mirrors range between 6.5°-13.5°. The slider mechanism has reliable performance after 6.9 billion cycles under continuous operation in vacuum (4mtorr).

## 1. INTRODUCTION

Micromirrors are becoming increasingly relevant for the MOEMS industry [1-12]. Numerous micromirrors actuated by PZT, thermal, magnetic, or electrostatic force have been demonstrated by using surface- or bulk-microfabrication processes. Usually, large scan angle and low drive voltage and current are desired to achieve high-resolution scanning, low power consumption and low-cost drive-electronics. We introduce the concept of the floating slider mechanism for electrostatic scanning mirrors to achieve these goals. This mechanism can amplify the mirror angular displacement from the movement of bimorph electrostatic actuators.

The prototype has been realized by using commercial foundries (MUMPs process) without costly customized fabrication processes. Furthermore, mirrors tilted via hinge linkages and bimorph structures do not require manual assembly, which is advantageous for reliability and practical manufacturing. The abrasive wear of the slider is a primary concern for long-term operation. A rough surface would act like a milling tool to remove material from the structure. Thus, a reliability test has been done in a vacuum chamber to check the abrasive wear.

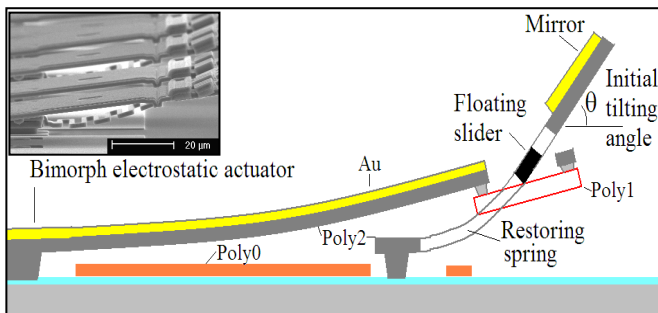


Figure 1: Schematic diagram of the scanning mirror with a preloaded floating slider mechanism to amplify angular movement. Upper left corner shows the SEM picture of the loaded restoring spring.

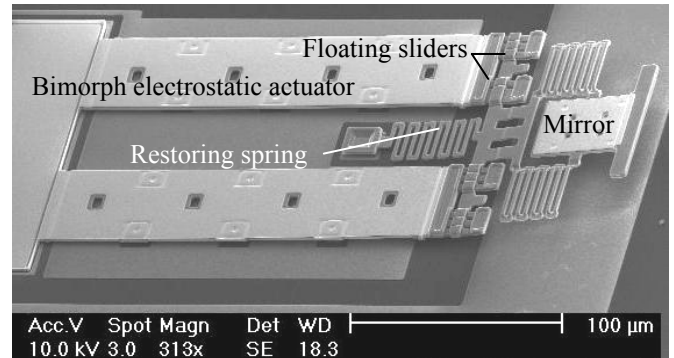


Figure 2: Dual bimorph electrostatic actuator with floating sliders.

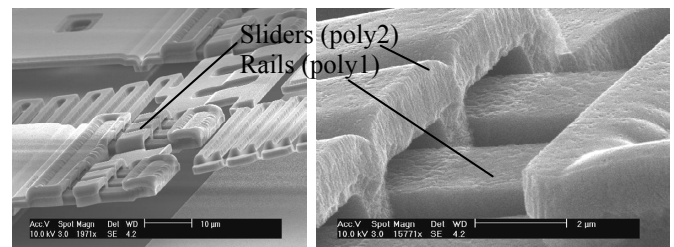


Figure 3 (a): The slider overlapped by Poly1 rails. These pictures were taken before testing.

Figure 3 (b): The Poly1 rails overlapped by Poly2 sliders. These pictures were taken before testing. The Poly2 sliders have rougher surface than uncovered Poly1 rails, due to the Poly2 masking of Poly1 to subsequent processes.

## 2. DESIGN AND PRINCIPLE

The schematic diagram of the scanning mirror is shown in Figure 1. The SEM picture is shown in Figure 2. A detailed feature of the floating slider before any testing is shown in Figure 3. The mirror is attached to the substrate via a restoring spring, which is driven by two curved gold-polysilicon bimorph electrostatic actuators through the floating-slider mechanisms. The size of the mirror is around  $30 \times 30 \mu\text{m}^2$ ; it is very small compared to most MEMS raster scan mirrors. Usually, large micromirrors are preferred for better scanning resolution. However, in this paper we are more interested in the wear of the slider mechanism under high resonance frequency. A smaller mirror with less mass is chosen to increase the mirror's natural frequency. After a 49% hydrofluoric acid and carbon dioxide

super-critical point release, the electrostatic actuator curls up by thermal residual stress from the MUMPs process. The flexures pull the mirror upward to the initial idle tilting angle. Tilting angles between  $6.5^\circ$ - $13.5^\circ$  are observed by different combinations of restoring springs, bimorph, and residual stress from the process, shown in Table 1. The initial tilting angle also presents the maximum static out-of-plane angular displacement for the mirrors, which is half of the maximum static optical scanning angle.

The sliding interface is located between the bottom surface of Poly2 and the top surface of Poly1. The roughness (RMS value measured by AFM) of the bottom surface of Poly2 and top surface of Poly1 is around 9.2 nm and 4.4nm, respectively. When voltage is applied, the electrostatic force of the flexures pulls the mirror downward. Since the restoring spring exerts a preload force on the bimorph that decreases the gap between the bimorph and the substrate, less voltage is required to drive it. The stored potential energy in the restoring spring contributes to the action. Compared to the potential energy required to deform torsion springs in other traditional continuous suspensions widely used in MEMS designs, the energy loss to friction in the slider is very small.

Table 1: Design and process parameters; the initial tilting angle is determined by residual stress and different combinations of restoring spring and bimorphs ( $W$ : width,  $L$ : length,  $T$ : tensile stress,  $C$ : compressive stress).

MUMPs RUN# / Design	Bimorph beam ( $\mu\text{m}$ )	Stress in Au/Poly2 (MPa)	Initial $\theta$
M51 /Type I	$W=50, L=200$	$T=35.5/C=7.5$	9.5
M44 / Type I	$W=50, L=200$	$T=16.0/C=6.5$	6.5
M44 / Type II	$W=50, L=400$	$T=16.0/C=6.0$	13.5

### 3. TESTING

Two different bimorph configurations with identical restoring spring and slider have been investigated; their parameters are shown in Table 1: Type II bimorph is two times longer than Type I. Figure 4 shows the measured static angular displacement of Type I and II at different voltages. The

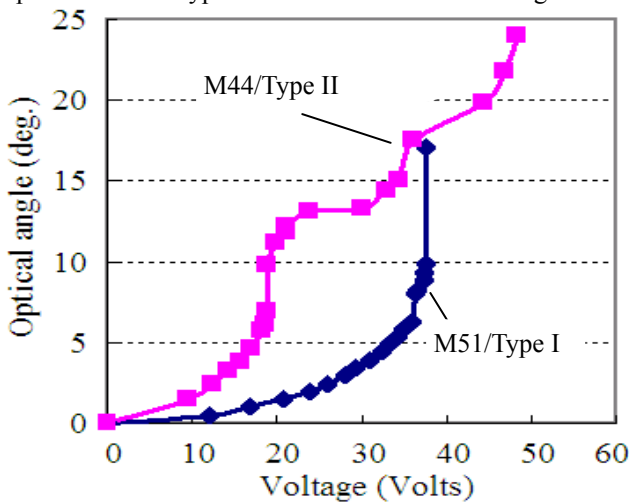


Figure 4: Static test results from Type I and Type II.

step-response in Type II is due to stepwise pull-in at each dimple on the underside of the bimorph. The dynamic response of the Type I scanning mirror in ambient air (Figure 5) shows two major resonance modes at 10.75kHz and

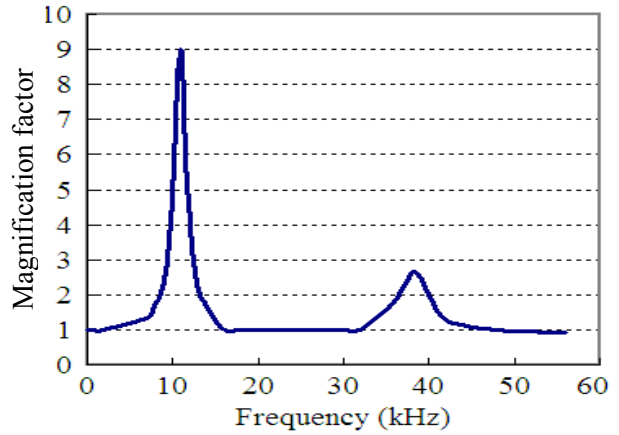


Figure 5: Normalized dynamic response of Type I.

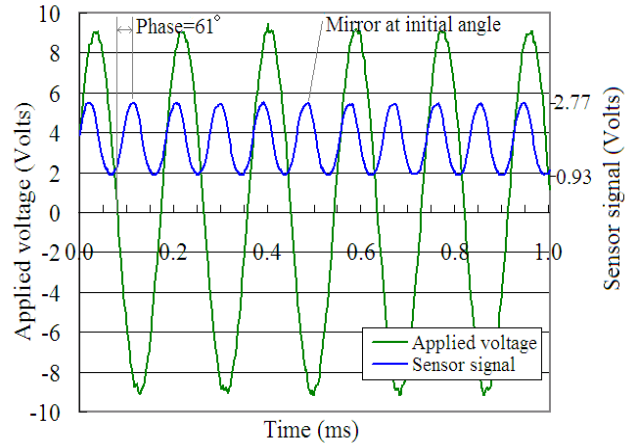


Figure 6: Sinusoidal excitation under natural frequency (Type I).

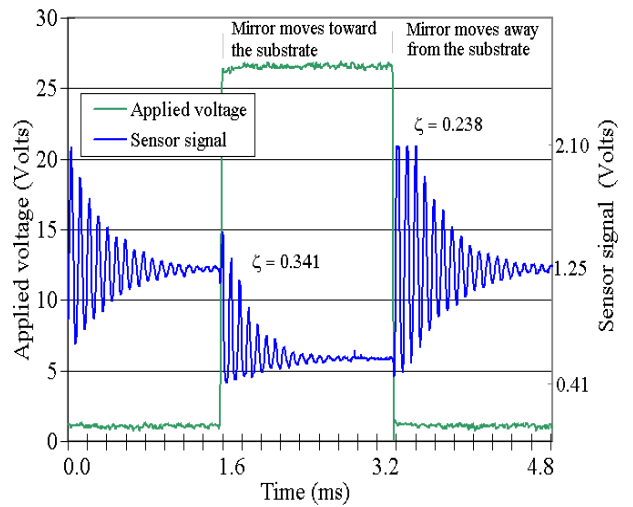


Figure 7: Transient response (Type I).

38.2kHz. The first resonance yields a maximum 17.8° scanning angle at  $V_{pp}=44.8V$  with the phase angle at  $-61^\circ$ . Figure 6 shows that the mirror motion with the floating slider mechanism can well reproduce the sinusoidal driving signal under resonance after  $6.9 \times 10^9$  cycles. The transient response has been investigated in the same environment by applying a 280Hz, 1.0-26.5V square wave signal (Figure 7). The damping ratio  $\zeta$  can be easily extracted from the curves. The system has a different damping ratio and settling time in charged and discharged states (Figure 7). When the mirror is charged and moved toward the substrate, the settling time (1.1ms, damping ratio = 0.341) is shorter than while moving away from the substrate (1.6ms, damping ratio = 0.238) due to the strong air damping effects in the small gap. The dynamic response of the mirror near the first resonance frequency also has been investigated in a vacuum chamber under different pressures (from 7mtorr to 10torr); the results are shown in Figures 8 and 9. The sliders still have reliable performance after 8-day continuous operation under resonance frequency of 10.2kHz. A comparison of these mirrors to some other published micromirrors [1-12] is listed in Figure 10. It shows that the electrostatic mirror made from MUMPs with floating

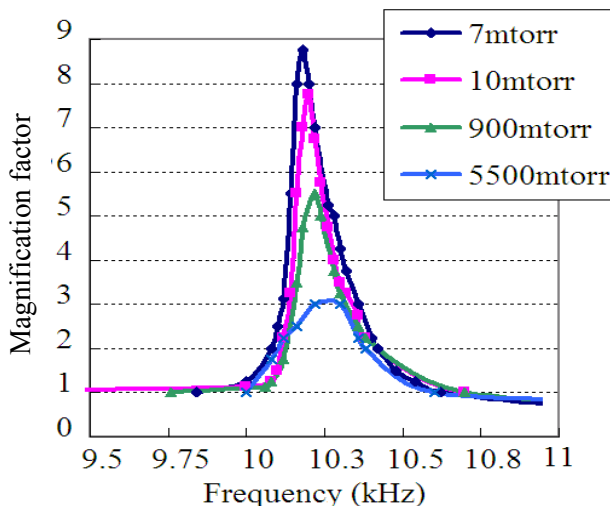


Figure 8: Dynamic response under different pressures (Type I).

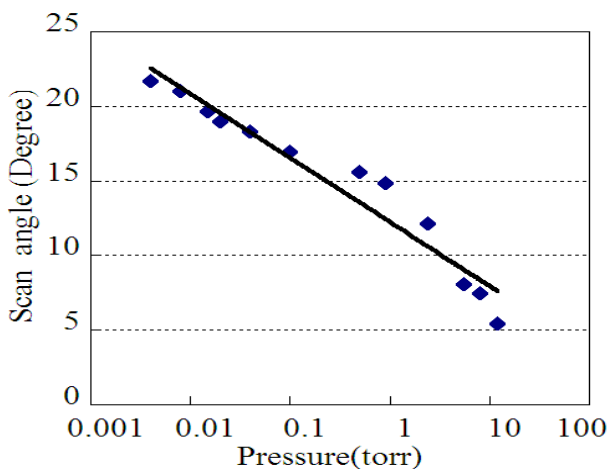


Figure 9: Maximum optical scan angle at resonance frequency under different pressures ( $V_{pp}=13.64V$ ).

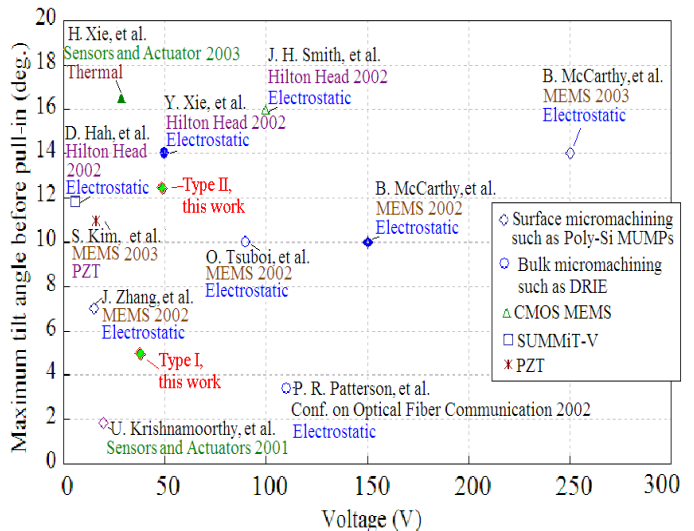


Figure 10: Scanning mirror comparisons: shape represents the processes, solid pattern means the actuator can pull mirror only in one direction. Low drive voltage and large tilt angle are desired for most of applications.

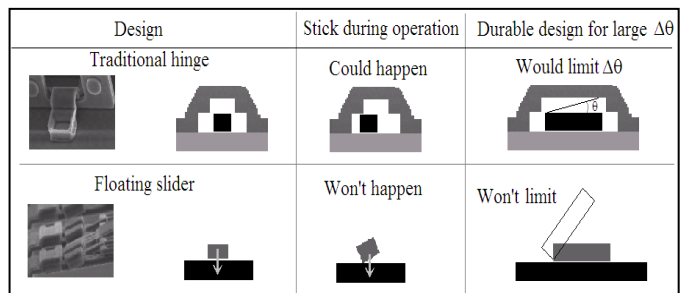


Figure 11: Comparisons between the traditional hinge and the floating slider.

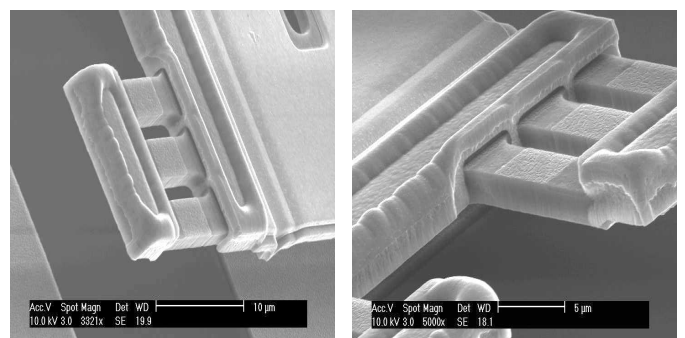


Figure 12: After 6.9 billion cycles, the slider has been removed for inspection. No significant abrasive wear has been found (Type I).

slider mechanism has similar or better performance compared to most other actuator technologies.

#### 4. DISCUSSIONS

Unlike other mechanisms with continuous suspensions that store potential energy during deformation, the floating mechanism is perfectly "soft", as it does not store any energy to achieve angular deflection. Thus, more of the preloaded

potential energy from thermal residual stress can be used to deform the soft restoring spring for a large initial tilt angle of the mirror. Mechanical wear would be the major concern for the reliability of the slider mechanism. Wear is unwanted removal of material through a sliding movement of a solid over another.

The wear rate is mainly determined by the surface hardness, roughness and contact pressure. Surface hardness and roughness are determined by the material and process. The contact pressure is a design parameter determined by the geometry of the slider and the rail. When the mirror is idle, the slider experiences the maximum contact pressure under static driving mode. Since the preloaded deflection ( $D$ ) is rather small compared to the length of the suspension beam ( $D < 0.2L$ ), it changes linearly with the preload force. The contact force can be calculated from the preload deformation and equivalent spring constant  $keq$  (1). It can be derived from [13]

$$keq = \frac{W(E_1^2 t_1^4 + E_2^2 t_2^4 + 2E_1 E_2 t_1 t_2 (2t_1^2 + 3t_1 t_2 + 2t_2^2))}{3(E_1 t_1 + E_2 t_2) L^3} \quad (1)$$

$$F = D Keq \quad (2)$$

where  $E_1$ ,  $E_2$ ,  $t_1$ ,  $t_2$  represent the Young's modulus and thickness of Gold and Poly2, respectively.  $L$  and  $W$  are the length and width of the bimorph. The preload displacement of M44/Type I is 9 $\mu$ m. The contact force can be calculated as 15.8  $\mu$ Nt.

Compared to traditional microhinges, floating slider designs provide both a large angular displacement and a durable structure (Figure 11). To verify the reliability of the floating-slider, testing has been performed in vacuum (4mtorr) to reduce the air damping effect. After  $6.9 \times 10^9$  continuous cycles under resonance at 6.1V, no significant abrasive wear has been observed (Figure 12). It should be noted that the tilt angle is also sensitive to thermal stress of the bimorph structure and working temperature. Changes in thermal residual stress from the process or from the temperature of the environment would affect the initial tilting angle of the mirror. Quality control of the process is critical for the performance and repeatability of the product.

## 5. CONCLUSIONS

This paper demonstrates the floating slider mechanism for a scanning mirror. The mirror can achieve large scanning angular displacements with low voltage. A designer can easily choose larger or wider sliders to reduce the contact pressure and achieve durable designs without losing the benefit of large angular displacement.

## REFERENCES

[1] H. Xie, Y. Pan, and G. K. Fedder, "Endoscopic optical coherence tomographic imaging with a CMOS-MEMS micromirror", *Sensors & Actuators A* 2003, pp. 237-241.

[2] B. McCarthy, V. M. Bright, and J. A. Neff, "A solder self-assembled torsional micromirror array", *IEEE MEMS* 2003, pp. 215-218.

[3] D. Hah, S. Huang, H. Nguyen, H. Chang, J. Tsai, M. C. Wu and H. Toshiyoshi, "Low voltage MEMS analog micromirror arrays with hidden vertical comb-drive actuators", *Hilton Head* 2002, pp.11-14.

[4] S. Kim, Y. Cho, H. Nam, and J. U. Bu, "Piezoelectrically pushed rotational micromirrors for wide angle optical switch applications", *IEEE MEMS* 2003, pp. 263-266.

[5] J. Kim, H. Lee, B. Kim, J. Jeon, J. Yoon, and E. Yoon, "A high fill-factor micro-mirror stacked on a crossbar torsion spring for electrostatically-actuated two-axis operation in large-scale optical switch", *IEEE MEMS* 2003, pp. 259-262.

[6] J. H. Smith, S. S. Nasiri, J. Bryzek, M. Novack, J. B. Starr, H. Kwon, A. F. Flannery, D. L. Marx, Z. Chen, and E. Sigari, "1200 mirror array integrated with CMOS for photonic switching: application of mechanical leveraging and torsional electrostatic actuation to reduce drive voltage requirements and increase angular tilt", *Hilton Head* 2002, pp. 378-379.

[7] J. Zhang, Y. C. Lee, V. M. Bright and J. Neff, "Digitally positioned micromirror for open-loop controlled applications", *IEEE MEMS* 2002, Las Vegas, pp. 536-539.

[8] Y. Xie and C. T. Nguyen, "A low-voltage tiltable microplatform using bent-beam actuation", *Hilton Head* 2002, pp. 329-332.

[9] B. McCarthy, V. M. Bright, and J. A. Neff, "A solder self-assembled large angular displacement torsional electrostatic micromirror", *IEEE MEMS* 2002, Las Vegas, pp. 499-502.

[10] O. Tsuboi, Y. Mizuno, N. Koma, H. Soneda, H. Okuda, S. Ueda, I. Sawaki and F. Yamagishi, "A rotational comb-driven micromirror with a large deflection angle and low drive voltage", *IEEE MEMS* 2002, Las Vegas, pp. 532-535.

[11] U. Krishnamoorthy, K. Li, K. Yu, D. Lee, J.P. Heritage, and O. Solgaard, "Dual-mode micromirrors for optical phased array applications", *Sensors & Actuators*, v. 97-98, 2001, pp. 21-26.

[12] P. R. Patterson, D. Hah, H. Nguyen, H. Toshiyoshi, R. Chao, and M. C. Wu, "A scanning micromirror with angular comb drive actuation", *Conference on Optical Fiber Communication, Technical Digest Series*, v.70, 2002, pp. 544-547.

[13] W.H. Chu, M. Mehregany and L. R. Mullen, "Analysis of tip deflection and force of a bimetallic cantilever microactuator", *J. Micromech. Microeng.* v3, 1993, pp. 4-7.